







Article

Biological Evaluation and Conformational Preferences of Ferrocene Dipeptides with Hydrophobic Amino Acids

Monika Kovačević ¹, Mojca Čakić Semenčić ^{1,*}, Ivan Kodrin ^{2,*}, Sunčica Roca ³, Jana Perica ¹, Jasna Mrvčić ⁴, Damir Stanzer ⁴, Krešimir Molčanov ⁵, Valentina Milašinović ⁵, Lidija Brkljačić ⁶ and Lidija Barišić ¹

- ¹ Department of Chemistry and Biochemistry, Faculty of Food Technology and Biotechnology, University of Zagreb, Pierottijeva 6, 10000 Zagreb, Croatia
- ² Department of Chemistry, Faculty of Science, University of Zagreb, Horvatovac 102a, 10000 Zagreb, Croatia
- ³ NMR Centre, Ruđer Bošković Institute, Bijenička cesta 54, 10000 Zagreb, Croatia
- ⁴ Department of Food Engineering, Faculty of Food Technology and Biotechnology, University of Zagreb, Pierottijeva 6, 10000 Zagreb, Croatia
- ⁵ Division of Physical Chemistry, Ruđer Bošković Institute, Bijenička cesta 54, 10000 Zagreb, Croatia
- ⁶ Division of Organic Chemistry and Biochemistry, Ruđer Bošković Institute, Bijenička cesta 54, 10000 Zagreb, Croatia
- * Correspondence: mojca.cakic@pbf.unizg.hr (M.Č.S.); ikodrin@chem.pmf.hr (I.K.); Tel.: +385-1-4605-067 (M.Č.S.); +385-1-4606-403 (I.K.)

Abstract: Despite the large number of peptidomimetics with incorporated heteroannularly functionalized ferrocenes, few studies have investigated their bioactivity. Here, we report the biological evaluation and conformational analysis of enantiomeric dipeptides derived from 1'-aminoferrocene-1-carboxylic acid (Fca) and hydrophobic amino acids (AA = Val, Leu, Phe). The conformational properties of Y-AA-Fca-OMe (Y = Ac, Boc) were elucidated by experimental (IR, NMR, CD, and X-ray) and theoretical (DFT) methods. The prepared dipeptides were screened for their antimicrobial activity against selected Gram-positive and Gram-negative bacteria, lactic acid bacteria and yeasts, while their antioxidant activity was tested by DPPH and FRAP methods. Of all compounds tested, dipeptide D-**2a** showed the best antibacterial properties against *S. aureus*, *B. subtilis*, and *P. aeruginosa* at a concentration of 2 mM. The time–kill curves showed that antibacterial activity was concentration- and time-dependent. Chirality (D-) and a more polar-protecting group (Ac) were found to affect the biological activity, both antimicrobial and antioxidant. All investigated peptides are considered to be highly hydrophobic and chemically stable in both acidic and buffer media. Dipeptides D-**1a–3a**, which showed biological activity, were subjected to the determination of proteolytic activity, revealing very good resistance to proteolysis in the presence of chymotrypsin.

Keywords: antimicrobial activity; antioxidant activity; proteolytic activity; chymotrypsin; hydrophobicity; peptidomimetics; conformational analysis; crystal structure; Density Functional Theory (DFT); hydrogen bonds



Citation: Kovačević, M.; Čakić Semenčić, M.; Kodrin, I.; Roca, S.; Perica, J.; Mrvčić, J.; Stanzer, D.; Molčanov, K.; Milašinović, V.; Brkljačić, L.; et al. Biological Evaluation and Conformational Preferences of Ferrocene Dipeptides with Hydrophobic Amino Acids. *Inorganics* **2023**, *11*, 29. <https://doi.org/10.3390/inorganics11010029>

Academic Editor: Lubov Snegur

Received: 2 December 2022

Revised: 22 December 2022

Accepted: 23 December 2022

Published: 3 January 2023



Copyright: © 2023 by the authors. Licensee MDPI, Basel, Switzerland. This article is an open access article distributed under the terms and conditions of the Creative Commons Attribution (CC BY) license (<https://creativecommons.org/licenses/by/4.0/>).

1. Introduction

Because of the ordered conformations that mimic natural peptide structures, researchers have investigated numerous amino acid derivatives of amino- and/or carboxyl-bis-functionalized ferrocenes over the past 30 years [1–7]. The restricted rotation of the ferrocene rings, caused by intramolecular hydrogen bonding between the peptide chains attached to the ferrocene moiety, results in helical and sheet structures that mimic naturally occurring secondary elements (Figure 1). To date, the most studied ferrocene peptidomimetics have been derived from 1'-aminoferrocene-1-carboxylic acid (Fca). It has been shown several times that the conformational space of these compounds can be fine-tuned by the number and type of constitutive amino acids, modification of their chirality,

and bulkiness of C- and N-protecting groups. In addition to their exceptionally well-defined conformational preferences, ferrocene peptides derived from Fca, as well as those with incorporated symmetrically disubstituted organometallic scaffolds ($-\text{OC}-\text{Fn}-\text{CO}-$ and $-\text{NH}-\text{Fn}-\text{NH}-$), have been used as protein-sensitive electrochemical probes [8,9], cation [10,11] and anion sensors [12], molecular receptors [13], chiroptic sensors [14], etc.

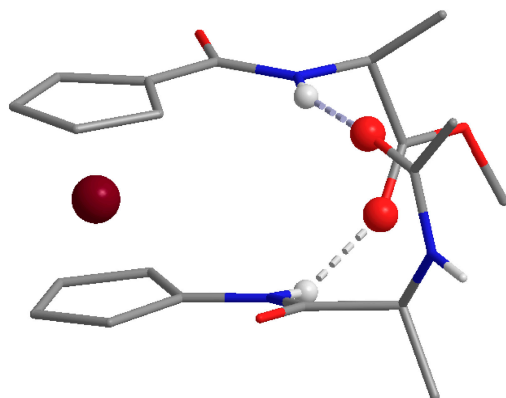


Figure 1. Turn structure in peptidomimetic Ac-Ala-Fca-Ala-OMe (non-polar hydrogens omitted for clarity) [4].

Scientific research in the biotechnology and pharmaceutical industries is focused on finding innovative antimicrobial compounds and antimicrobial mechanisms, as well as alternatives to traditional antibiotics in response to antimicrobial resistance. Small antimicrobial peptides (AMPs) with antimicrobial activity are the subject of interest among scientists. In natural sources, bioactive peptides are usually present in low concentrations, which makes their isolation and purification difficult. Therefore, chemical synthesis is often performed to obtain appropriate amounts for the proper peptide. The preparation of ferrocene bioconjugates with antimicrobial peptides proved to be a good potential strategy in the search for more selective and less toxic antimicrobial drugs, the use of which would reduce the overuse of antibiotics and thus the increasing and ubiquitous antimicrobial resistance [15]. Costa et al. coupled ferrocene molecules with the RP1 peptide derived from the human chemokine CXCL4 to investigate how this modification alters the structure, biological activity, and toxicity of the peptide [16]. The results suggest that ferrocene increases antimicrobial activity against the Gram-positive bacterium *S. agalactiae*. The Fc-RP1 peptide also decreased the minimum inhibitory concentration (MIC) in assays against *E. faecalis* ($\text{MIC} = 7.9 \mu\text{mol L}^{-1}$), *E. coli* ($\text{MIC} = 3.9 \mu\text{mol L}^{-1}$), and *S. aureus* ($\text{MIC} = 3.9 \mu\text{mol L}^{-1}$). Wenzel et al. reported the antibiotic properties of hetero tri-organometallic compounds with ferrocene and showed potent antibacterial activity against Gram-positive bacteria [17]. It was active against *S. aureus* strains, including MRSA and VISA strains, in the low micromolar range, comparable to antibiotics. They identified the bacterial membrane as the target of the antibiotic. MIC values were $1.4 \mu\text{M}$ for *B. subtilis* and *S. aureus*, but no inhibition of *E. coli* and *P. aeruginosa* growth was observed. Ardila-Chantre et al. synthesized and characterized short-peptide conjugates of buforin and lactoferricin B using ferrocene as modifiers, resulting in higher antibacterial activity than the original unconjugated peptides [18]. Slootweg et al. synthesized ferrocene-containing lysine peptides with excellent antimicrobial activity in the low micromolar range [19].

Khelef and Lanez measured the antioxidant activity of ferrocene derivatives containing amine, amide, and hydrazine groups via the DPPH method [20]. Their results indicate that ferrocene derivatives scavenge DPPH radicals, and the activity is strongly dependent on the presence of a nitrogen atom in the molecule. Milaeva et al. showed that the antioxidant activity of ferrocene containing 2,6-di-*tert*-butylphenol or phenyl groups strongly depends on the presence of a phenolic group but is enhanced in the presence of the ferrocenyl fragment [21]. Štimac et al. synthesized a series of homoannularly and heteroannularly

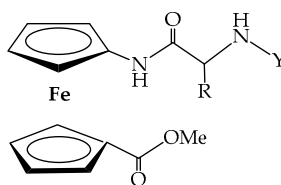
substituted adamantyl ferrocene derivatives, which showed antioxidant activity in the DPPH assay and protected the cell membrane from peroxidation [22].

The applicability of peptides for therapeutic use is usually determined by their low membrane permeability and high proteolytic degradation [23]. To achieve their satisfactory permeability through the phospholipid bilayer, various optimization strategies are employed, including the insertion of unnatural amino acids, modification of the side-chain or backbone, amidation or acetylation as terminus protection, and cyclization of peptides [24]. Li et al. showed that ferrocene conjugated to the pentapeptide KLVFF [25] and to the tripeptide GPR [26] exhibited improved lipophilicity and significant resistance to proteolytic degradation compared to its parent peptide, thanks to incorporating the lipophilic and enzymatically stable ferrocene moiety.

Conventional peptides, consisting of amino acid residues, are rapidly degraded by proteases. The specificity of chymotrypsin for the hydrolysis of peptide bonds formed by the carboxyl groups of Tyr, Phe, Trp, and Leu is well known, and therefore this enzyme was chosen to test the stability of ferrocene dipeptides [27]. Amides with unnatural backbones are very resistant to proteolytic cleavage [28], so one can assume that ferrocene amino acid plays an important role in the stabilization of dipeptides by enzymatic cleavage.

Although many organic compounds and natural products with incorporated ferrocene units [29] have been investigated as potential drugs [30] due to the desirable properties of ferrocene (non-toxicity, stability, and lipophilicity), the literature on the bioactivity of 1,1'-disubstituted ferrocene peptides is very limited. To date, only a few studies on their biological activity have been performed, most of them carried out by our group to provide a guide for the development of potential drug candidates [6,31–33]. Unfortunately, conjugates with the incorporated $-\text{NH}-\text{Fn}-\text{CO}-$ template [Y-Fca-Pro-OMe (**I**, Y = Ac, Boc), Y-Pro-Fca-OMe (**II**, Y = Ac, Boc), and homo- and heterochiral Y-Pro-Ala-Fca-OMe (**III**, Y = Ac, Boc)] showed no or rather modest antiproliferative activity on MCF-7 and HeLa cell lines. Exceptions are the heterochiral Boc-D-Pro-L-Ala-NH-Fn-COOMe, which has a moderate potential to promote apoptotic cell death of HeLa cells, and Ac-Ala-Fca-Ala-OMe, which shows prominent cytotoxic activity against human breast and liver cancer cells. Somewhat weaker cytotoxic effects on Hep G2 and Hs 578 cells were elicited by conjugates **IVa**, Ac-Ala-NH-Fn-NH-Ala-Boc, and **IVb**, Fn-(NH-Ala-Ac)₂, which are derived from the ferrocene-1,1'-diamine scaffold. Through the in vitro evaluation of compounds **I–IV**, we found that the crucial factor determining the bioactivity of the tested compounds is their lipophilicity. Considering the close relationship between lipophilicity and hydrophobicity of amino acids [34,35], in our recent work [36], we replaced Ala in peptides **IVa** by amino acids with hydrophobic bulky side chains to prepare both enantiomeric pairs of homochiral derivatives Ac-AA-NH-Fn-AA-Boc (**V**, AA = Phe, Val, Leu) and to test their antitumor, antimicrobial, and antioxidant activities. The cytotoxicity tests performed on HeLa, HepG2, and MCF-7 cell lines revealed only weak antitumor activity of the peptidomimetics **V**, while the antimicrobial activity tested by the disk diffusion method was not observed. All prepared compounds showed moderate antioxidant activity in the rank of 0.1 mM Trolox equivalent, determined by the DPPH method, and in the range of 0.52–0.63 mM Trolox, evaluated by the FRAP method.

Although the peptidomimetics **V** did not show antimicrobial activity, initial tests of the inhibitory potential of the compounds Y-D-AA-Fca-OMe (Y = Ac, Boc; AA = Phe, Val, Leu), the precursors of the D-series of **V**, were encouraging. Based on these results and the lack of data on the antioxidant activity of ferrocene peptidomimetics, we report here a detailed study of Y-AA-Fca-Ome (Figure 2). The conformational properties of the synthesized peptides were studied by spectroscopic (IR, NMR, and CD), DFT, and crystallographic analyses. For their biological evaluation, hydrophobicity and proteolytic stability were studied, followed by measurement of the antimicrobial and antioxidant activity (DPPH and FRAP methods).



L- and D-**1a** (R = CH(CH₃)₂, Y = COCH₃) L- and D-**1b** (R = CH(CH₃)₂, Y = COOC(CH₃)₃)
 L- and D-**2a** (R = CH₂CH(CH₃)₂, Y = COCH₃) L- and D-**2b** (R = CH₂CH(CH₃)₂, Y = COOC(CH₃)₃)
 L- and D-**3a** (R = CH₂C₆H₅, Y = COCH₃) L- and D-**3b** (R = CH₂C₆H₅, Y = COOC(CH₃)₃)

Figure 2. Ferrocene dipeptides with hydrophobic amino acids.

2. Results and Discussion

Details of the synthesis and spectroscopic and spectrometric characterization data of compounds L-/D-**1a–3a** and L-/D-**1b–3b** are reported in [36]. We note that details not described in [36] can be found in the Supplementary Materials (Table S1, Figures S1–S6).

2.1. Infrared (IR), Nuclear Magnetic Resonance (NMR) and Circular Dichroism (CD) Studies

As mentioned in the Introduction, amino acid derivatives of heteroannularly substituted ferrocenes are usually stabilized with intramolecular hydrogen bonds (IHBs), both in solution and in the solid state. To investigate whether the dipeptides L-/D-**1a–3a** and L-/D-**1b–3b** adopt ordered conformations supported by IHBs in solution, we performed IR, NMR, and CD spectroscopic studies. Since the enantiomeric pairs of the target compounds have identical chemical and physical scalar properties, the experimental IR and NMR data are reported for the D-series only. The amide region of the solution IR spectra of compounds D-**1a–3a** and D-**1b–3b**, shown in Figure 3, is dominated by the medium-intensity blue-shifted signals of the non-bonded NH groups, accompanied by lower-intensity bands below 3440 cm⁻¹ assigned to the associated NH groups. The unchanged ratio of these signals when diluted from $c = 5 \times 10^{-2}$ M to 3×10^{-3} M excludes the possibility of intermolecular hydrogen bonding under these conditions and shows a higher fraction of conformers with non-bonded NH groups (Figures S7–S12).

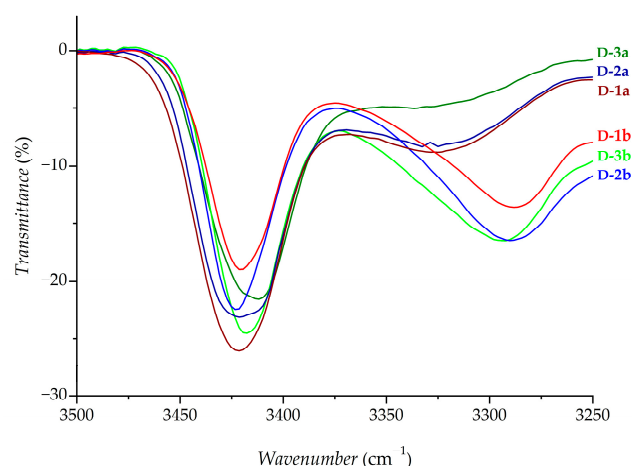


Figure 3. The NH region of the FTIR spectra of D-**1a–3a** and D-**1b–3b**.

To address the question of which NH groups of D-**1a–3a** and D-**1b–3b** are involved in IHBs, we performed an NMR study focusing on the amide proton resonances, allowing us to estimate whether the respective NH group is involved in hydrogen bonding [4–6]. A possible aggregation at higher concentrations, leading to a downfield shift of the NH signals, was investigated by concentration-dependent NMR experiments of compounds D-**1a–3a** (Table S2). The relatively small change in resonances ($\Delta\delta \leq 0.63$ ppm) during dilution from 50 to 6 mM concentrations suggests that the initial shifts in NH protons are

mainly due to the IHBs. As can be seen in Table 1, in the NMR spectra of all derivatives, the high chemical shift of the NH_{Fca} group ($\delta > 7$ ppm) indicates the involvement of this group in hydrogen bonding, especially in the case of the Ac-protected derivatives D-1a–3a. It can be assumed that the NH_{AA} group of derivatives D-1a–3a, which was found in a higher field (~ 6.5 ppm), oscillates between free and hydrogen-bonded states. Although the *N*-terminal NH groups of D-1b–3b resonate at high fields, the possibility of intramolecular hydrogen bonding cannot be ruled out, as urethan amide protons have been shown to occur in a number of peptides at high fields [37,38].

Table 1. Chemical shifts [δ /ppm] of the NH protons of D-1a–3a and D-1b–3b in $\text{CDCl}_3\text{-}d$ ($c = 5 \times 10^{-2}$ M).

	δ (ppm)					
	D-1a	D-1b	D-2a	D-2b	D-3a	D-3b
NH_{Fca}	8.19	7.38	8.15	7.62	7.73	7.32
NH_{AA}	6.46	5.15	6.38	5.03	6.44	5.15

The strength of IHBs involving NH groups was estimated by recording temperature- and solvent-dependent NMR spectra of derivatives D-1a–3a. The temperature dependence of chemical shifts of NH_{Fca} and NH_{AA} over the temperature range of 258–328 K is shown in Figure 4a, and the data are listed in Table S3. Large temperature coefficients of NH_{Fca} ($\Delta\delta/\Delta T = -16.86, -15.43,$ and -14.14 ppb/K for D-1a, D-2a, and D-3a, respectively) and NH_{AA} ($\Delta\delta/\Delta T = -7.86, -11.28$ and -9.14 ppb/K for D-1a, D-2a, and D-3a, respectively) indicate that these groups participate in weak hydrogen bonds that are perturbed as the temperature increases [39]. These findings are in close agreement with the results of the DMSO- d_6 titration experiments (Figure 4b and Table S4). Increasing the percentage of a strong hydrogen bond acceptor from 0% to 55% in $\text{CDCl}_3\text{-}d$ caused a strong perturbation of the chemical shifts of NH_{Fca} and NH_{AA} of derivatives D-1a–3a ($\Delta\delta = 1.44\text{--}1.87$ ppm), further confirming the involvement of these groups in weak IHBs.

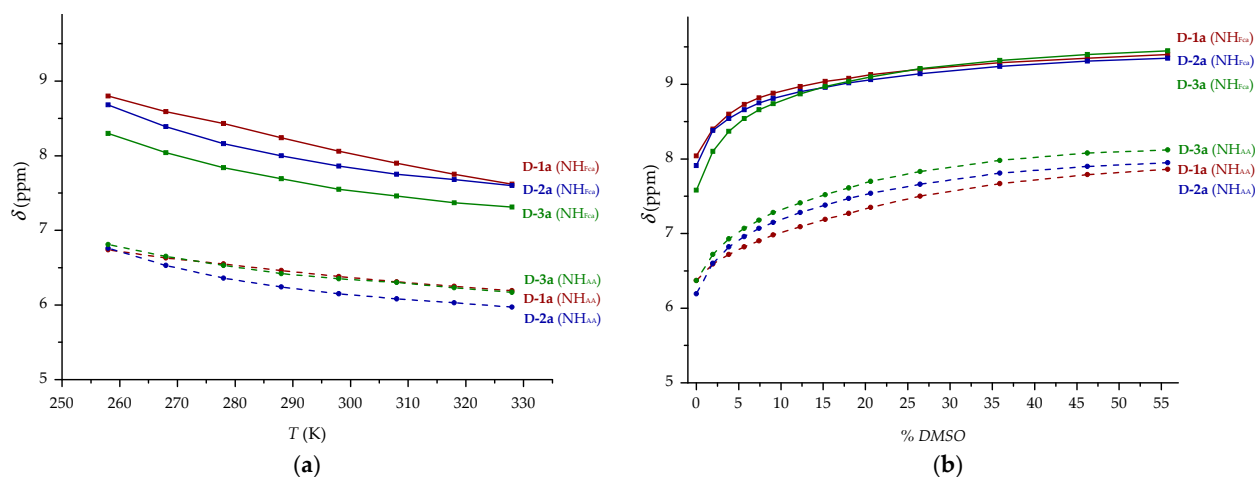


Figure 4. (a) Temperature dependence of the amide proton chemical shifts for D-1a–3a. (b) Solvent dependence of the amide proton chemical shifts of D-1a–3a while increasing concentrations of DMSO- d_6 in $\text{CDCl}_3\text{-}d$.

Finally, to investigate whether these weak IHBs cause the chiral perturbation of the ferrocene chromophore, the circular dichroism (CD) spectra of all derivatives were measured. The signals near 470 nm in the CD spectra of the ferrocene peptides are induced by the chiral environment of the organometallic chromophore. The CD activity, which originates from the central chirality of the constituent amino acids, is usually very weak [40], while the restriction of the rotation of the ferrocene rings induced by interchain IHBs causes

strong Cotton effects ($\theta > 5000 \text{ deg cm}^2 \text{ dmol}^{-1}$). The medium- and low-intensity signals are characteristic of monosubstituted ferrocene peptides, stabilized by intrachain IHBs [41,42], and derivatives whose conformational space contains multiple available, energetically accessible conformations [4,43,44]. As expected, the visible region of CD spectra of the enantiomeric peptides L-/D-**1a–3a** and L-/D-**1b–3b**, shown in Figure 5, contains mirror-image curves. The L-chirality of the constituent amino acids leads to positive CD signals of low intensity and vice versa (Table S5).

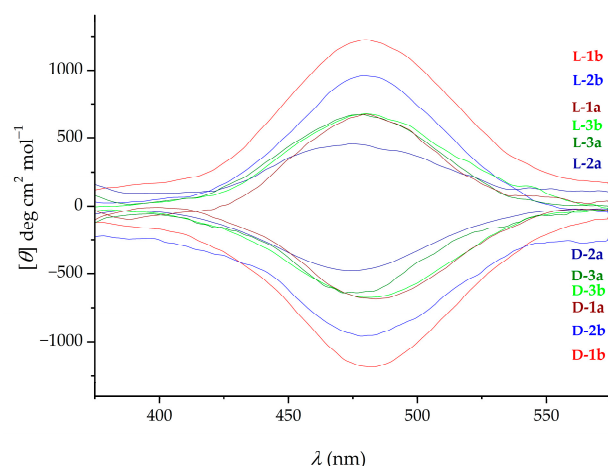


Figure 5. CD spectra of L-/D-**1a–3a** and L-/D-**1b–3b** in CH_2Cl_2 ($c = 1 \times 10^{-3} \text{ M}$).

The results of IR, NMR, and CD analyses of the dipeptides L-/D-**1a–3a** and L-/D-**1b–3b** are consistent with previous reports of similar types of “short” ferrocene peptides [4,42,43], which are best described as an ensemble of interconverting conformations stabilized by intra- and interchain IHBs.

2.2. Computational Study

To better understand the conformational preferences in simple ferrocene peptidomimetics and explain the most common intramolecular hydrogen bonding patterns, we commonly rely on a hierarchical approach to computational modeling [6,31,36,41–51]. A relatively fast Monte Carlo conformational analysis resulted in the first set of conformers suitable for further optimizations at higher levels of theory in the implicitly modeled solvent. The final step involves the verification of hydrogen bonds using Bader’s quantum theory of atoms in molecules (QTAIM) analysis and Koch and Popelier’s criteria. Further details can be found in the Computational details section.

Conformational analysis was performed only for the D-series of Ac-protected **1a–3a** and Boc-protected **1b–3b** derivatives (Figure 6 and Table S6). We expect the same Boltzmann distribution and hydrogen bonding patterns for each pair of enantiomers. Because of the relatively short substituents consisting of only one *N*-protected amino acid (Val, Leu, or Phe) on the first cyclopentadienyl ring and an ester group (COOMe) on the second cyclopentadienyl ring, hydrogen bonds can only form between the two potential hydrogen bond donors (NH_{Fca} and NH_{AA}) and the two hydrogen bond acceptors ($\text{O}=\text{C}_{\text{Ac/Boc}}$ and $\text{O}=\text{C}_{\text{COOMe}}$), since the third acceptor $\text{O}=\text{C}_{\text{AA}}$ is too close to both NH groups to form a hydrogen bond. The conformational analysis revealed the existence of several hydrogen-bonding patterns (Figure 5, bottom). The first pattern **A**, consisting of two hydrogen-bonded rings (a 7-membered $\text{NH}_{\text{Fca}} \cdots \text{OC}_{\text{Ac}}$ and a 9-membered $\text{NH}_{\text{AA}} \cdots \text{OC}_{\text{COOMe}}$), is more common in Ac-protected derivatives of **1a–3a** where *P*-helicity predominates in the lowest energy conformers, with the $\text{O}=\text{C}_{\text{Ac/Boc}}$ group pointing toward the NH_{Fca} group. In contrast, Boc-protected **1b–3b** derivatives show mostly *M*-helicity, where $\text{O}=\text{C}_{\text{Ac/Boc}}$ oxygen points away from the NH_{Fca} group, leaving only a 9-membered ring ($\text{NH}_{\text{AA}} \cdots \text{OC}_{\text{COOMe}}$), which is additionally strengthened by the short 5-membered ring ($\text{NH}_{\text{Fca}} \cdots \text{N}_{\text{AA}}$) as in pattern **B**. Each

ensemble shows relatively close energy states with different hydrogen bonding patterns and helicities, so a direct comparison with the experimental results is not straightforward.

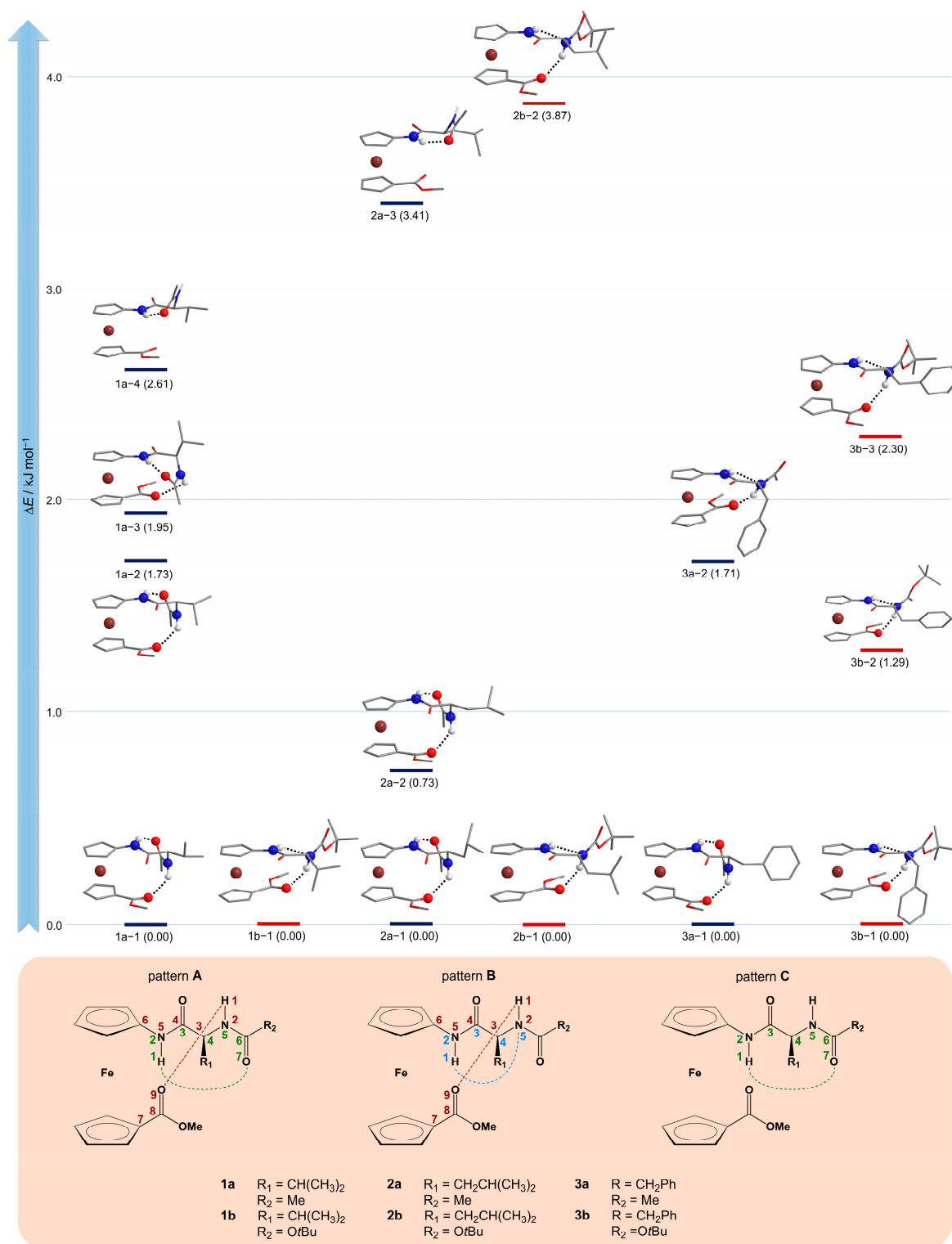


Figure 6. The most stable conformers of D-series of **1a–3a** Ac-protected (blue horizontal lines) and **1b–3b** Boc-protected (red horizontal lines) optimized at the B3LYP-D3/6-311+G(d,p) (LanL2DZ for Fe) level of theory; SMD model used for solvent effect calculations. Nonpolar hydrogen atoms are omitted for clarity. Dashed lines represent hydrogen bonds verified by the QTAIM analysis. Hydrogen-bonding patterns and the numbering schemes of the n -membered hydrogen-bonded rings.

The results presented here are in perfect agreement with our previous studies on very similar ester systems with alanine (Y-Ala-Fca-OMe; Y = Ac, Boc) [43] and acetyl systems with glycine, alanine, and valine (Y-AA-Fca-Me; Y = Ac, Boc; AA = Gly, Ala, Val) [44]. In both studies, the disubstituted Fca derivatives also show the same hydrogen bonding patterns among the most stable conformers, with no specific preference for one type of helicity over another. Relatively low intensities of the signals in the CD spectra near 470 nm in all these studies may indicate the simultaneous presence of several energetically relatively close conformers of opposite helicities.

2.3. X-ray Crystal Structure Analysis

Compound D-2a crystallizes with $Z' = 2$, i.e., with two symmetry-independent molecules per asymmetric unit (Figure 7). These molecules labelled A and B adopt similar conformations (Figure S13), with the main difference being the orientation of the carboxymethyl group (C19 in A and C39 in B), which is rotated 180° in two conformers. However, these molecules do not exhibit the protein-like “twist” conformation shown in Figure 1. Instead, the conformations of A and B are “open” and have no intramolecular hydrogen bonding. However, there is an extensive network of intermolecular hydrogen bonding (Table S7) with four symmetry-independent N–H···O and four weaker C–H···O bonds. Of these, five connect molecules A and B within the asymmetric unit, whereas the other three link different asymmetric units to form a 3D network (Figure 8). It is likely that this multitude of hydrogen bonds stabilizes the “open” conformation.

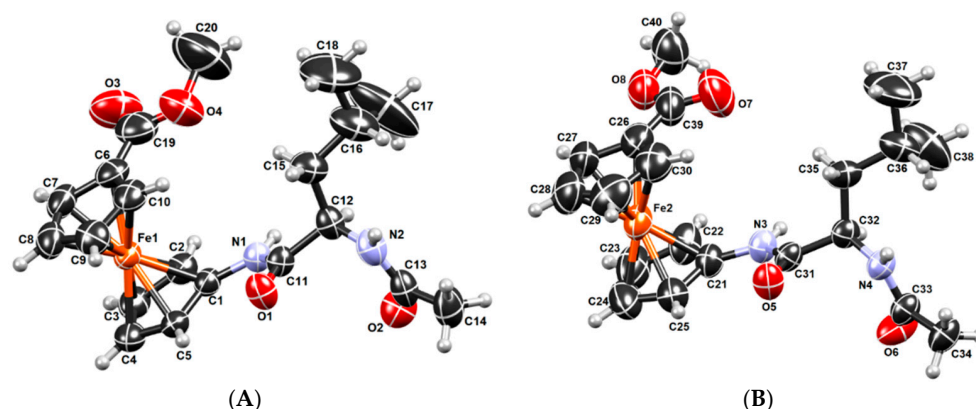


Figure 7. ORTEP-3 [52] drawings of two symmetry-independent molecules of D-2a with atom numbering scheme: (A,B) Displacement ellipsoids are drawn for the probability of 50% and hydrogen atoms are shown as spheres of arbitrary radii.

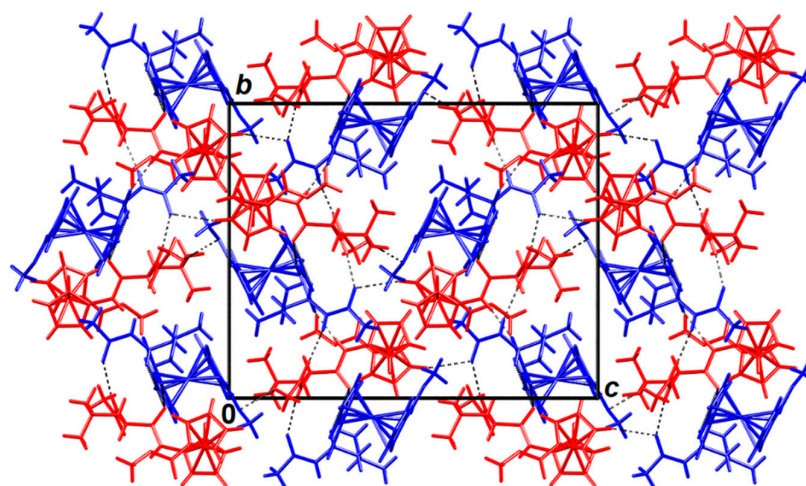


Figure 8. Crystal packing of D-2a viewed in the direction [100]. Molecule A is red and B is blue, and hydrogen bonds are shown as black dashed lines.

Indeed, the “open” conformations are not found among the most stable conformers, as shown by the computational study of **2a**. We have already explained this effect by calculating interaction energies for similar systems in our previous study [42]. The energy penalty connected to the reorganization of the most stable conformer (stabilized by *intramolecular* hydrogen bonds) into the less favorable open conformation is overcome by the network of *intermolecular* hydrogen bonds between molecules in the crystal.

2.4. Biological Evaluation

2.4.1. Antimicrobial Activity

The antimicrobial activity of the target compounds was evaluated against Gram-positive and Gram-negative bacteria, lactic acid bacteria, and yeasts using a disk diffusion method, microdilution methods, and colony counting methods. Their antioxidant activity was evaluated by the 1,1-diphenyl-2-picryl-hydrazyl radical scavenging method and the ferric-reducing antioxidant power method.

The antimicrobial activity of ferrocene peptides was preliminarily tested by the disk diffusion method. Of the 12 compounds tested, compounds **D-1a**, **D-2a**, and **D-3a** showed antimicrobial activity with inhibition zones of 7–19 mm against the bacteria *P. aeruginosa*, *B. subtilis*, and *S. aureus* (Figure 9, Table 2). The absence of a growth inhibition zone around the diagnostic disks indicates the resistance of the other tested bacteria, lactic acid bacteria, and yeasts to these ferrocene peptides. The other tested compounds also did not show antimicrobial activity in all tested microorganisms despite the high concentrations (1 mg of the compound was applied to the disk). Compound **D-2a** showed the strongest antimicrobial activity, especially against the bacterium *P. aeruginosa*. Compound **D-3a** showed the same antimicrobial activity against the three mentioned bacteria, while compound **D-1a** showed very weak inhibition and only against *B. subtilis*. The mentioned ferrocene dipeptides cause the appearance of inhibition zones but only when the bacterial cells were treated with high concentrations of the compounds (Table 2). Their antimicrobial activity was significantly weaker than that of the antibiotic kanamycin, which was used as a positive control, and at a much lower concentration (Figure 9).

Table 2. Growth inhibition zones of the tested microorganisms and minimum inhibitory concentrations (MIC) of the tested compounds **D-1a**, **D-2a**, and **D-3a**.

Compound	Test Microorganisms	Molarity of Solutions for Disk Diffusion Method (mM)	Inhibition Zone (mm)	MIC (mM)
D-1a	<i>S. aureus</i>		nd	>2
	<i>B. subtilis</i>	251	7 ± 1	>2
	<i>P. aeruginosa</i>		nd	>2
D-2a	<i>S. aureus</i>		16 ± 1	>2
	<i>B. subtilis</i>	243	16 ± 1	>2
	<i>P. aeruginosa</i>		19 ± 2	>2
D-3a	<i>S. aureus</i>		14 ± 1	>2
	<i>B. subtilis</i>	224	14 ± 1	>2
	<i>P. aeruginosa</i>		14 ± 1	>2
Kanamycin	<i>S. aureus</i>		25 ± 0	nd
	<i>B. subtilis</i>	50 µg disk	25 ± 0	nd
	<i>P. aeruginosa</i>		28 ± 1	nd

nd—not detected.

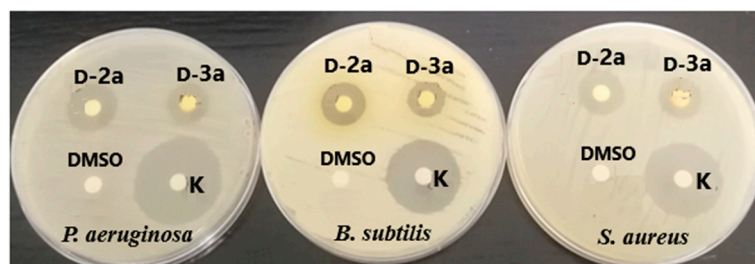


Figure 9. Inhibition zone of D-2a and D-3a against *P. aeruginosa*, *B. subtilis*, and *S. aureus* (D-2a, D-3a—1 mg/disk; K—Kanamycin 50 μ g disk—positive control, DMSO—negative control).

In view of the preliminary results, further studies of antimicrobial activity were performed only for compounds D-1a, D-2a, and D-3a and the bacteria whose growth was inhibited by the mentioned compounds. Microdilution methods were performed to determine the minimum inhibitory concentrations. Due to the poor solubility of the synthesized compounds in water, which is an essential component of culture media for the growth of microorganisms, the compounds were dissolved in a DMSO solution. DMSO alone in concentrations greater than 2% also inhibited the growth of bacterial species (results not shown). Thus, the highest possible concentrations of the synthesized ferrocenes that could be tested were 2 mM. These concentrations were applied and were not found to be sufficient for bacteriostatic activity. In fact, the optical density measurements indicated growth of the tested bacterial species in the presence of 2 mM of the tested compounds. Since the measured optical densities were slightly lower compared to the control, the colony-counting method was used to describe the antimicrobial activity of the peptides of interest more accurately. The results showed that the number of bacterial cells growing in the presence of 2 mM of compound D-2a for 24 h was lower by one decimal dilution for all three bacterial species tested (Figure 10).

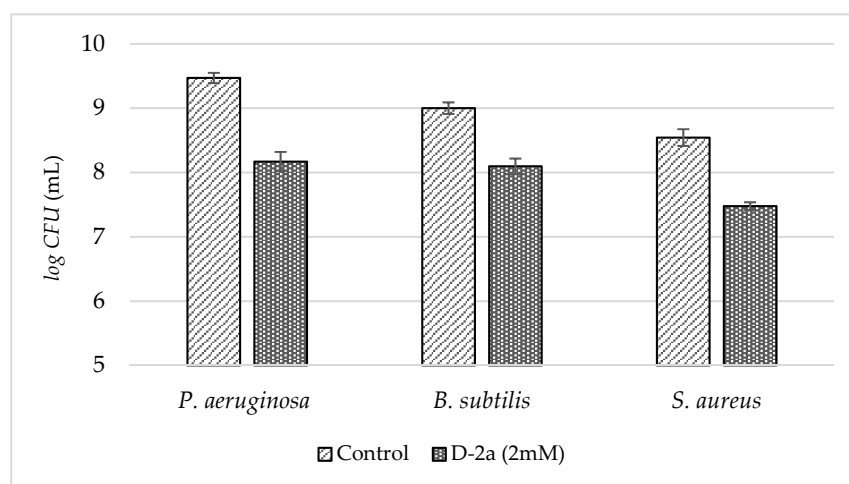


Figure 10. Bacterial density expressed as log CFU/mL of *S. aureus*, *B. subtilis*, and *P. aeruginosa* after 24 h of incubation without (control) and 2 mM of compound D-2a. Each column and bar represent the mean and the standard deviation, respectively ($n = 2$). CFU, colony-forming unit.

In addition, time–kill curves were generated for compound D-2a and the bacterium *P. aeruginosa*, which was most sensitive to the effect, allowing the growth of microorganisms to be followed as a function of time and the antimicrobial concentration. Different concentrations in the range of 0–2 mM were used. Curves in the presence (killing curves) and absence (growth curves) of compound D-2a were compared (Figure 11). There were no significant differences in the growth curves of *P. aeruginosa* when exposed to different concentrations of the test compound ($p > 0.05$). However, some effects of antimicrobial activity can be seen. At an inhibitory concentration of 2 mM, there is a minimal change in

CFU levels in the first three hours compared to the control. At both 2 mM and 1 mM, the difference in CFU levels was most pronounced after 8 h. The time–kill assay showed that the inhibitory effect of the test compound on *P. aeruginosa* was concentration-dependent. There was little difference between the time–kill curves of the bacteria at 0.5 mM and the control. After 8 h, the number of viable bacteria decreased at 1 mM and 2 mM in one and two decimal dilutions, respectively. At the end of the experiment (24 h), the cells in the kill curves (2 mM) were almost the same size as the cells in the growth curves, and the difference had decreased to one decimal dilution.

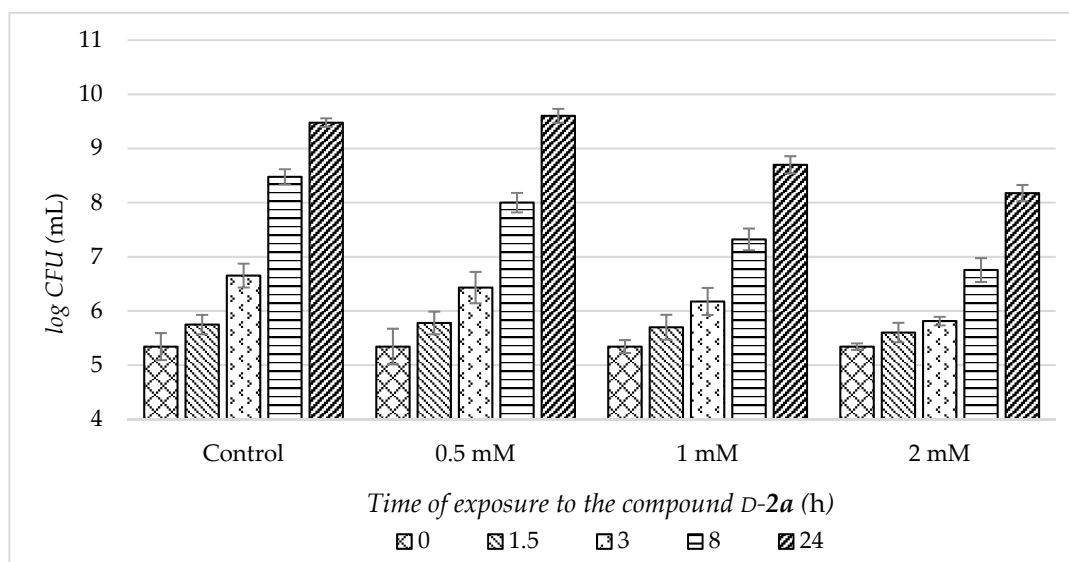


Figure 11. Bacterial density expressed as log CFU/mL of *P. aeruginosa* at baseline and after 1.5 h, 3 h, 8 h, and 24 h of incubation without (control) and in the presence of 0.5 mM, 1 mM, and 2 mM of compound D-2a. Each column and bar represent the mean and standard deviation, respectively ($n = 2$). CFU, colony-forming unit.

We report the antimicrobial activity of twelve synthesized ferrocene bioconjugates against selected bacteria and yeasts, three of which showed antimicrobial activity at relatively high concentrations ranging from 224 to 251 mM. It can be seen that the compounds were active against two bacterial species from the group of Gram-positive and Gram-negative bacterial species, while antimicrobial activity against the group of lactic acid bacteria and yeasts was completely absent. This does not indicate that the compounds are more active against any particular group of bacteria. As can be seen, the MIC values obtained with the ferrocene bioconjugate listed in the Introduction [16] are much lower than the 2 mM tested for compounds D-2a and D-3a, which reduced the growth of *S. aureus*, *B. subtilis*, and *P. aeruginosa* by two and one decimal dilutions after eight and 24 h, respectively (Figure 11). These differences may be attributed to the poor solubility of our peptides in water and culture media (in contrast to the water-soluble bioconjugates of ferrocene synthesized by Costa et al. [16]). Poor water solubility is one of the problems cited as a disadvantage for the clinical application of AMP, along with other factors such as poor selectivity, hemolytic activity and host toxicity, and low stability to protease degradation in vivo [53].

2.4.2. Antioxidant Activity

The antioxidant activity of ferrocene compounds was measured by the 1,1-diphenyl-2-picrylhydrazyl (DPPH) and ferric-reducing antioxidant power (FRAP) methods. Results are reported as mM Trolox for the FRAP method and mM Trolox equivalent for the DPPH method. Results were compared using 0.5 mM Trolox as the reference substance (Table 3) and visually displayed as a principal component analysis (PCA) score plot (Figure 12). Both D-1a–3a and D-1b–3b peptides showed higher antioxidant activity measured by the FRAP

method, whereas peptides L-1a–3a showed the lowest antioxidant activity measured by both methods.

Table 3. Antioxidative activity of ferrocene compounds evaluated using free 1,1-diphenyl-2-picrylhydrazyl radical scavenging assay and ferric-reducing antioxidant power methods.

Compound (1 mM)	DPPH (% Inhibition)	DPPH (mM Trolox Equivalent)	FRAP (mM Trolox)
L-1b	11.75 ± 2.10	0.150	2.16 ± 0.013
L-2b	16.55 ± 1.77	0.211	2.27 ± 0.006
L-3b	5.50 ± 3.87	0.067	1.62 ± 0.001
D-1b	7.76 ± 0.65	0.099	2.17 ± 0.015
D-2b	8.79 ± 2.10	0.112	2.21 ± 0.003
D-3b	3.99 ± 0.48	0.051	2.00 ± 0.001
L-1a	4.57 ± 0.64	0.058	0.58 ± 0.009
L-2a	3.19 ± 1.29	0.041	0.72 ± 0.004
L-3a	3.65 ± 2.26	0.046	1.09 ± 0.030
D-1a	10.62 ± 1.13	0.135	2.29 ± 0.003
D-2a	6.96 ± 0.81	0.089	1.77 ± 0.001
D-3a	5.25 ± 2.26	0.067	2.22 ± 0.006
Standard (0.5 mM Trolox)	39.27 ± 8.40	0.500	

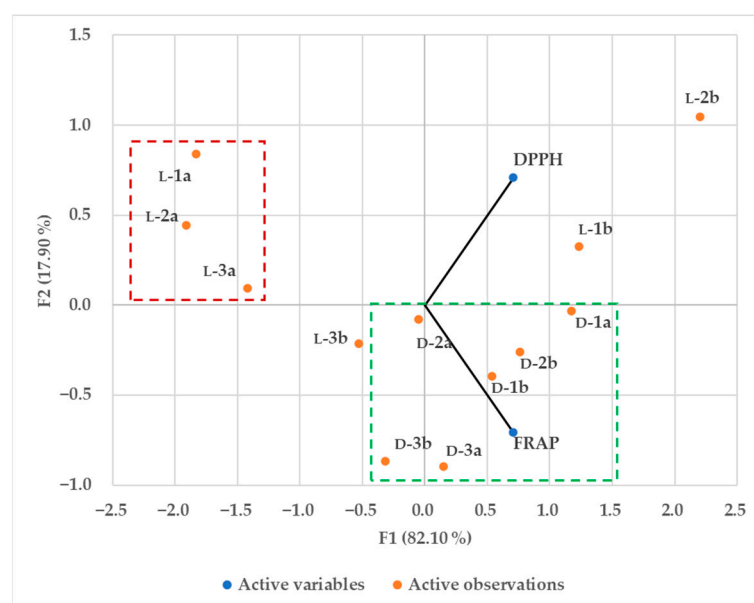


Figure 12. Principal component analysis (PCA) plot of different dipeptides based on their antioxidant activity; highlighted in green—dipeptides with D-amino acids and higher antioxidant activity; highlighted in red—dipeptides with L-amino acids and acetyl as the protecting group with the lowest antioxidant activity.

In our previous work [36], we also showed that homochiral conjugates of ferrocene-1,1'-diamine with L-/D-Phe, L-/D-Val, and L-/D-Leu exhibited moderate antioxidant activity in the range of 0.1 mM Trolox equivalent evaluated by the DPPH method and in the range of 0.52–0.63 mM Trolox evaluated by the FRAP method, which is in the range of antioxidant activity of the compounds synthesized in this work (Table 3). Zhang et al. summarized compounds that are important ROS scavengers, including peptides and poly(amino)-based ROS scavengers [54]. They pointed out sulphur-containing amino acids (e.g., cysteine, cystine, and methionine), aromatic amino acids (e.g., tyrosine, tryptophan, phenylalanine), proline, and histidine as relatively strong ROS scavengers, which is not

consistent with our results, as compounds with Phe (D-**3a,b**, L-**3a,b**) did not show stronger antioxidant activity (Figure 12).

2.5. Hydrophobicity

There are several features that are important for antimicrobial activity, such as peptide hydrophobicity, net charge, amphipathic nature, and secondary structure [55,56]. Inter alia, the hydrophobicity of peptides is a crucial factor responsible for hydrophobic interactions with the hydrophobic core of the phospholipid bilayer, causing membrane disruption, cytoplasm leakage, and possibly cell death [57]. Of the twelve dipeptides tested, only those with a more polar acetyl group and D-amino acids (D-**1a–3a**) showed antibacterial activity.

To determine how the applied amino acid and *N*-terminal protection (Boc/Ac) affect the overall hydrophobicity of the derived dipeptides, elution from the column was tested with acetonitrile (ACN). As described in the Introduction, ferrocene is known to be a highly lipophilic component, making its bioconjugates more efficiently permeable through the phospholipid bilayer. The hydrophobic amino acids (Val, Leu, and Phe) present in the target compounds with ferrocene render all the derived dipeptides highly hydrophobic, so it is predictable that a high percentage of acetonitrile will be required to elute the dipeptides from the column. Since the C18 stationary phase (used for the measurement) is nonpolar and the mobile phase (water-acetonitrile) is polar, longer retention times (t_R) should correlate with higher hydrophobicity of the compounds [58–61]. Peptides with a Boc-protecting group L-**1b–3b** and D-**1b–3b** showed higher hydrophobicity compared to compounds with a more polar Ac-protecting group (L-**1a–3a** and D-**1a–3a**) (Figure S14).

For passive diffusion through a phospholipid-bilayer, it is important to find a middle ground between hydrophobicity/hydrophilicity of the designed peptide (hydrophobic enough to interact with the nonpolar lipid chains in the phospholipid bilayer but not too lipophilic to be trapped in the membrane or insoluble in water) [23,62,63]. This could be the reason why bioconjugates with acetyl protection showed antimicrobial activity against *P. aeruginosa*, *B. subtilis*, and *S. aureus*. The retention time and percentage of ACN for compounds with the same protecting group at the *N*-terminus increased due to the increased hydrophobicity of the amino acid residues used. The absolute configuration at the α -carbon atom of the α -amino acids did not affect the hydrophobicity of the peptides with the same protecting group at the *N*-terminus (Table 4).

Table 4. List of the peptides used in the study. The abbreviation, retention time (t_R), and percentage of acetonitrile (% ACN) at elution are displayed.

Compound	t_R /min	% ACN
L- 1b	7.1	82.6
L- 2b	8.3	87.5
L- 3b	8.3	87.9
D- 1b	7.1	82.6
D- 2b	8.3	87.5
D- 3b	8.3	87.9
L- 1a	2.6	63.7
L- 2a	3.3	66.6
L- 3a	3.6	68.0
D- 1a	2.6	63.7
D- 2a	3.3	66.6
D- 3a	3.6	68.0

2.6. Proteolytic Stability of Ferrocene Peptides

The chemical stability of ferrocene peptides was studied in 0.1 M PBS buffer as a degradation assay in neutral (pH 7.4) and 0.045% TFA as a degradation assay in acidic media (pH 3.0). D-**1a** was most degraded in 0.045% TFA within 24 h, 48.8% compared to the original response, and 64.9% and 63.6% compared to D-**2a** and D-**3a**, respectively. In the buffer, the compounds are stable and show no significant degradation (Figure 13).

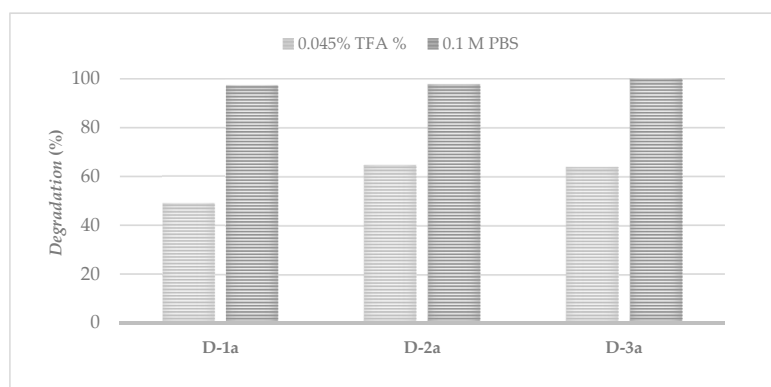


Figure 13. Percentage of degradation of ferrocene peptides in 0.045% TFA and 0.1 M buffer after 24 h.

The results agree with previous studies showing the degradation of ferrocene in an acidic medium [16,64]. Our dipeptides are more stable in buffer media, as shown by the work of Costa and al. [16] in terms of the percentage of degradation of their peptides, which can be up to 100%. The results of the three acetyl-protected dipeptides (D-1a–3a), which are not affected in the buffer media, are of importance because the proteolytic stability tests are performed at pH 7.4. To test the proteolytic stability of the compounds with the greatest potential microbial activity, i.e., D-1a–3a, the same RP-HPLC-UV analysis was used as in the determination of stability in buffer and in acid.

Since chymotrypsin preferentially cleaves peptides at the carboxyl side of bulky hydrophobic residues, it is expected to cause the most severe degradation of the D-3a dipeptide, followed by the derivative that is degraded less preferentially in the presence of chymotrypsin, D-2a. After 24 h of incubation with the enzyme, D-1a showed significant stability without enzymatic conversion, suggesting that chymotrypsin does not recognize the peptide bond adjacent to valine as a potential cleavage site.

D-3a showed an 18.7% decrease in peak area, whereas D-2a decreased by 6% (Figure 14). Although chymotrypsin selectively hydrolyzes the peptide bond at the phenylalanine and leucine residues, the dipeptides are highly resistant to proteolysis. The results of Chen et al. [27] show that the interplay of disulfide bonds, α -helicity, and hydrophobic interactions enhances the proteolytic activity of the dimeric peptides used. Hydrogen bonds contribute favorably to protein stability, and even when the polar groups are not hydrogen bonded, they can contribute favorably to protein stability [65]. As we pointed out in the Introduction, the incorporation of unnatural backbones into peptides as well as the introduction of D-amino acids makes the derived compounds highly resistant to proteolytic cleavage [28,66], so it can be concluded that ferrocene amino acid (Fca) in combination with D-amino acid plays an important role in the stabilization of dipeptides by enzymatic degradation.

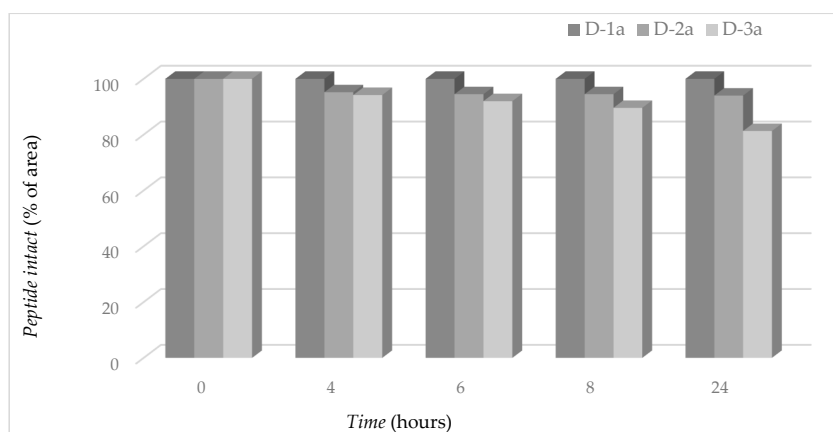


Figure 14. Proteolytic stability of ferrocene peptides during 24 h.

3. Materials and Methods

3.1. Conformational Analysis

The ferrocene dipeptides were synthesized as precursors of more complex peptides published in our most recent paper [36]. The Supplementary Materials contains the synthetic procedures and spectroscopic characterization of L-/D-**1a–3a** and L-/D-**1b–3b** [36]. The infrared spectra were recorded as CH₂Cl₂ solutions between NaCl windows using a Perkin Elmer Spectrum Two spectrophotometer. The NMR spectra were recorded using a Bruker AV600 spectrometer (Bruker BioSpin GmbH, Rheinstetten, Germany) at the Ruđer Bošković Institute. A 5-mm broadband probe head with z-gradient coils operating at 600.130 MHz for ¹H and 150.903 MHz for ¹³C was used. Recorded spectra were referenced to the residual solvent peak (CDCl₃-*d*, ¹H: δ = 7.24 ppm, ¹³C: δ = 77.23 ppm). When the CDCl₃-*d*/DMSO-*d*₆ mixture was used, calibration was performed using Me₄Si as an internal standard (¹H: δ = 0.0 ppm). NMR titrations were performed by adding 10 μ L DMSO-*d*₆ to NMR tubes containing 25 mM CDCl₃-*d* solutions of the dipeptides. Spectra were recorded after each addition, and DMSO-*d*₆ was added until no change in the chemical shift of the amide protons was observed. CD spectra were recorded using a Jasco-810 spectropolarimeter in CH₂Cl₂. Molar ellipticity coefficients (θ) are in degrees, the concentration *c* is in molL⁻¹, and the path length *l* is in cm, so the unit for (θ) is deg cm² dmol⁻¹.

3.2. Computational Details

The conformational analysis was performed in three steps. The first step involved The Monte Carlo Multiple Minimum and Mixed torsional/Low-mode sampling with molecular mechanics (OPLS2005 force field) in MacroModel [67,68]. The most stable conformers were optimized at a high level of theory (B3LYP/LanL2DZ) in Gaussian16 [69] with default convergence criteria and, finally, at the B3LYP-D3/6-311+G(d,p) level of theory (LanL2DZ basis set on Fe) [70–72] in the implicitly modeled chloroform as a polarizable continuum [73]. Each geometry was confirmed to be a true minimum on the potential energy surface. The relative energies reported are for the standard Gibbs free energies at 298 K. The hydrogen-bonding patterns were analyzed using Bader's QTAIM theory in the AIMAll program [74]. The presence of hydrogen bonds between the selected hydrogen bond donors and acceptors was confirmed by comparing the calculated topological parameters at the bond critical points with the values proposed by Koch and Popelier [75].

3.3. X-ray Diffraction

Single-crystal diffraction data were collected with a Rigaku Oxford Diffraction Synergy S four-circle diffractometer (Rigaku Oxford Diffraction Ltd., Yarnton, UK) using microfocus CuK α radiation. Data reduction and multi-scan data collection were performed using the CrysAlis PRO version 1.171.42.69a program package [76]. The structure was solved using direct methods from SHELXS97 [77] and refined using SHELXL-2017 [78] within the WinGX program package [79]. All non-hydrogen atoms were refined anisotropically using full-matrix least-squares refinement. For the hydrogen atoms, the riding model was used. The PLATON program [80] was used to calculate the molecular geometry, and molecular graphics were created using ORTEP-3 [50] and Mercury [81]. Crystallographic and refinement data for the structures reported in this work are listed in Table S8.

3.4. Antimicrobial Activity

Microorganisms: Gram-positive bacteria (*Staphylococcus aureus*, *Bacillus subtilis*, *Enterococcus faecium*, and *Listeria monocytogenes*), Gram-negative bacteria (*Pseudomonas aeruginosa*, *Escherichia coli*, and *Salmonella enterica* s. Typhimurium), lactic acid bacteria (*Leuconostoc mesenteroides* and *Lactobacillus plantarum*), and yeasts (*Candida albicans*, *Candida utilis*, *Rhodotorula sp.*, and *Saccharomyces cerevisiae*) were used to evaluate the antimicrobial properties of the tested peptides. The microorganisms were stored on slant agar in the microorganism collection of the Laboratory of General Microbiology and Food Microbiology and

the Laboratory of Fermentation and Yeast Technology of the Faculty of Food Technology and Biotechnology, University of Zagreb (Croatia).

Antimicrobial disk diffusion testing: The disk diffusion method was used to preliminarily test the efficacy of the samples on all strains tested. The disk diffusion method is a common method for pretesting the antimicrobial activity of potential antimicrobial compounds. For this reason, and because the detailed description of the work was included in our previous manuscript [36] and is repeated identically here, we do not discuss it in detail in this manuscript.

Determination of MIC: The minimum inhibitory concentration (MIC) was determined spectrophotometrically using the broth microdilution method [82]. Briefly, Mueller–Hinton broth was used for bacterial growth. Fresh 24-h broth culture was used (*S. aureus*, *B. subtilis*, *P. aeruginosa*), and the final density was set at 1×10^5 CFU/mL. Twofold dilution series of the test compound (D-1a, D-2a, and D-3a) were prepared in 200 μ L of the medium. The compound was tested in a concentration gradient of 2–0.125 mM. During the experiment, a growth control without the test compound, kanamycin as a positive control, and the compound (stained) in the medium without microorganisms as a negative control were maintained. The microtiter plate was incubated at 37 °C for 24 h, after which the optical density was measured. The minimum concentration of the test substance that completely inhibits bacterial growth is referred to as the MIC.

Time–kill curve determination: The broth macrodilution method was used to generate a time–kill curve against *P. aeruginosa*. Briefly, for the time–kill curve, compound D-2a was evaluated at different multiples of tentative MIC—2 mM ($\frac{1}{4} \times$ MIC, $\frac{1}{2} \times$ MIC, and MIC). Three milliliters of Mueller–Hinton broth containing the appropriate concentration of the test compound were inoculated for 24 h for freshly grown *P. aeruginosa* to obtain a final concentration of 105 colony-forming units per mL. All test tubes were incubated at 37 °C in a thermostat, and samples were taken from each test tube after 0, 1.5, 3, 8, and 24 h. To determine the number of live cells, serial tenfold dilutions were prepared in sterile saline and aseptically spread on Mueller–Hinton agar plates. All agar plates were incubated at 37 °C for 24 h, and colonies were counted to determine colony-forming units per mL. The time–kill curve was constructed by plotting log 10 of colony-forming units per mL against time.

3.5. Antioxidant Activity Assays

Methods for determining antioxidant activity are based on the study of a reaction in which a free radical is generated and inhibited by the addition of the sample whose antioxidant activity is measured. The antioxidant activity of the tested peptides ($c = 1$ mM) is determined using the radical scavenger DPPH and the antioxidant power of ferric ions (FRAP). A detailed description of the work was also included in our previous manuscript [36] and is repeated identically here.

3.6. Statistical Analysis

Statistical analysis was performed with the MS Excel tool XLStat (Addinsoft, Paris, France) program. The data shown are mean values ($n = 2$). Differences between control and dipeptide microbial groups were subjected to analysis of variance (ANOVA). Principal component analysis (PCA) was used to visualize differences between dipeptides based on their antioxidant activity.

3.7. Hydrophobicity

Hydrophobicity of the dipeptides was measured by RP-HPLC-UV at 215 nm (Agilent Technologies 1200 series HPLC-DAD-MS/MS; Agilent Technologies Inc., Palo Alto, CA, USA) on a Zorbax XDP C18 column (75×4.6 mm², 3.5 μ m particle size) (Agilent Technologies Inc.). The solvents for the analysis were 95% 0.1% TFA in water + 5% ACN (solvent A) and 95% ACN + 5% 0.1% TFA in water (solvent B). The gradient was applied as follows: 0 min 50% B, 0–10 min 50% B–100% B, 10.1–13 min 100% B, 13.1–18 min 50% B. The flow

rate was 0.5 mL/min. Samples were prepared as 100 µg/mL solution in acetonitrile. The injection volume was 10 µL. The percentage of B eluent was read on the instrument for the retention time of each ferrocene peptide and corrected for the percentage of water in the B eluent.

3.8. Chemical Stability

Analysis was performed on RP-HPLC-UV at 215 nm (Agilent Technologies 1200 series HPLC-DAD-MS/MS) on a Zorbax XDP C18 column (75 × 4.6 mm², 3.5 µm particle size) (Agilent Technologies Inc.) by observing the decrease in the peak area of samples prepared in buffer and in TFA immediately after preparation and 4 h, 6 h, 8 h, and 24 h after preparation. The solvents for the analysis were 95% 0.1% TFA in water + 5% ACN (solvent A) and 95% ACN + 5% 0.1% TFA in water (solvent B). The gradient was applied as follows: 0 min 30% B, 0–10 min 30% B–100% B, 10.1–13 min 100% B, 13.1–18 min 20% B. The flow rate was 0.5 mL/min [16,58,59]. The stock solution of peptides with the greatest potency against microbial activity (D-1a–3a) was prepared as a 10 mg/mL solution in ACN. The dilution was prepared in 0.1 M buffer or 0.045% TFA as a 200 µg/mL solution. Samples were analyzed immediately after preparation and 4, 6, 8, and 24 h after sample preparation.

3.9. Proteolytic Stability

To test the proteolytic stability of the compounds, the same RP-HPLC-UV analysis was performed as in the determination of stability in the buffer and in acid. Samples were prepared as a 200 µg/mL solution in 0.1 M PBS with the addition of 26.3 µg/mL chymotrypsin. Peak area was measured immediately after preparation and 4 h, 6 h, 8 h, and 24 h after sample preparation. The curves of degradation were plotted as the percentage of intact peptide measured by the analysis of peak area as a function of time.

4. Conclusions

Here, we report the antimicrobial activity of 12 synthesized compounds against selected Gram-positive and Gram-negative bacteria, lactic acid bacteria, and yeasts, as well as their antioxidant activity. The compounds with antimicrobial activity (D-1a, D-2a, and D-3a) against *P. aeruginosa*, *B. subtilis*, and *S. aureus* were selected by the disk diffusion method and compared with kanamycin as a positive control. Using the colony-counting method, dipeptide D-2a at the highest concentration tested (2 mM) was found to inhibit bacterial growth at a decimal dilution after 24 h. Time–kill curves, which have the advantage of providing more detailed information on the timing and progression of antibacterial activity, showed that antibacterial activity was concentration- and time-dependent, and the best antimicrobial activity was observed after 8 h of exposure to the compound. Chirality (D-amino acids) and polarity of the protecting group (acetyl) were found to affect the biological activity, as dipeptides D-1a–3a showed better antimicrobial activity compared to the other dipeptides tested. Chirality also affects antioxidant activity. Dipeptides with D-amino acids showed higher antioxidant activity as measured by the FRAP method, while compounds with L-amino acids and acetyl as the protecting group showed the lowest antioxidant activity. A different effect of two protecting groups (Ac vs. bulkier Boc) on the biological activity of the studied peptides is also roughly indicated by the results of conformational analysis. A change in the protecting group on the N-terminus leads to different hydrogen bonding patterns in the solution and results in various molecular landscapes available for specific interactions with biological systems. The results of the conformational analysis of the studied dipeptides are in perfect agreement with previous reports on similar types of “short” ferrocene peptides, which are best described as an ensemble of interconverting energetically close conformers with opposite helicities.

Moreover, many synthetically produced peptides are not considered bioavailable due to proteolytic degradation by gastrointestinal enzymes. The stability of D-1a–3a in the presence of chymotrypsin proved to be remarkably high, even when the natural substrates of the enzyme (Leu and Phe) were used.

Therefore, the prepared dipeptides could provide a good template for the development of new ferrocene peptides with enhanced biological activity and bioavailability.

Supplementary Materials: The following supporting information can be downloaded at: <https://www.mdpi.com/article/10.3390/inorganics11010029/s1>, Table S1: Melting points of L-/D-**1a-3a** and L-/D-**1b-3b**; Figure S1: HRMS spectrum of compound D-**1a**; Figure S2: HPLC spectrum of compound D-**1a**; Figure S3: HRMS spectrum of compound D-**2a**; Figure S4: HPLC spectrum of compound D-**2a**; Figure S5: HRMS spectrum of compound D-**3a**; Figure S6: HPLC spectrum of compound D-**3a**; Figure S7: The NH stretching vibrations in concentration-dependent IR spectra of D-**1b** in DCM; Figure S8: The NH stretching vibrations in concentration-dependent IR spectra of D-**2b** in DCM; Figure S9: The NH stretching vibrations in concentration-dependent IR spectra of D-**3b** in DCM; Figure S10: The NH stretching vibrations in concentration-dependent IR spectra of D-**1a** in DCM; Figure S11: The NH stretching vibrations in concentration-dependent IR spectra of D-**2a** in DCM; Figure S12: The NH stretching vibrations in concentration-dependent IR spectra of D-**3a** in DCM; Table S2: Concentration dependence of NH chemical shifts of derivatives D-**1a**, D-**2a** and D-**3a**; Table S3: Temperature dependence of chemical shifts of ferrocene peptides D-**1a**, D-**2a** and D-**3a**; Table S4: DMSO titration of ferrocene peptides D-**1a**, D-**2a** and D-**3a**; Table S5: UV/Vis-signals and Cottons effects in peptides L-/D-**1a-3a** and L-/D-**1b-3b**; Table S6: Relative energies (reported energies refer to standard Gibbs free energies at 298 K in kJ mol^{-1}) of the most stable conformers of D-series of compounds **1a-3a** (Ac-protected) and **1b-3b** (Boc-protected), AA = Val, Leu, Phe; Figure S13: Overlay of two symmetry-independent molecules in crystal structure of D-**2a**; Table S7: Geometric parameters of hydrogen bonding; Table S8: Crystallographic, data collection and refinement data; Figure S14: HPLC chromatograms of L-/D-**1a-3a** and L-/D-**1b-3b**.

Author Contributions: Conceptualization, M.K., M.Č.S. and I.K.; methodology, M.K., L.B. (Lidija Barišić), J.M., M.Č.S. and I.K.; software, I.K.; validation, M.K., S.R., I.K., J.M., D.S., K.M., V.M. and L.B. (Lidija Brkljačić); investigation, M.K., S.R., I.K., J.M., D.S., K.M., V.M., J.P. and L.B. (Lidija Brkljačić); writing—original draft preparation, M.K., J.M., L.B. (Lidija Barišić), K.M., M.Č.S. and I.K.; writing—review and editing, M.K., M.Č.S. and I.K.; supervision, L.B. (Lidija Barišić); project administration, L.B. (Lidija Barišić); funding acquisition, L.B. (Lidija Barišić). All authors have read and agreed to the published version of the manuscript.

Funding: This work has been fully supported by the Croatian Science Foundation under the project IP-2020-02-9162.

Data Availability Statement: The crystallographic data have been deposited in the Cambridge Structural Database as entries no. 2223686. The DFT, spectroscopic, and biological evaluation data are provided as figures and tables and are included in this paper.

Acknowledgments: Computational resources were provided by the Isabella cluster at Zagreb University Computing Centre (SRCE).

Conflicts of Interest: The authors declare no conflict of interest.

References

1. Herrick, R.S.; Jarret, R.M.; Curran, T.P.; Dragoli, D.R.; Flaherty, M.B.; Lindyberg, S.E.; Slate, R.A.; Thornton, L.C. Ordered conformations in bis(amino acid) derivatives of 1,1'-ferrocenedicarboxylic acid. *Tetrahedron Lett.* **1996**, *37*, 5289–5292. [[CrossRef](#)]
2. Kirin, S.I.; Wissenbach, D.; Metzler-Nolte, N. Unsymmetrical 1, n' -disubstituted ferrocenoyl peptides: Convenient one pot synthesis and solution structures by CD and NMR spectroscopy. *New J. Chem.* **2005**, *29*, 1168–1173. [[CrossRef](#)]
3. Barišić, L.; Rapić, V.; Metzler-Nolte, N. Incorporation of the Unnatural Organometallic Amino Acid 1'-Aminoferrocene-1-carboxylic Acid (Fca) into Oligopeptides by a Combination of Fmoc and Boc Solid-Phase Synthetic Methods. *Eur. J. Inorg. Chem.* **2006**, *20*, 4019–4021. [[CrossRef](#)]
4. Čakić Semenčić, M.; Siebler, D.; Heinze, K.; Rapić, V. Bis- and Trisamides Derived From 1'-Aminoferrocene-1-carboxylic Acid and α -Amino Acids: Synthesis and Conformational Analysis. *Organometallics* **2009**, *28*, 2028–2037. [[CrossRef](#)]
5. Chowdhury, S.; Mahmoud, K.A.; Schatte, G.; Kraatz, H.-B. Amino acid conjugates of 1,1'-diaminoferrocene. Synthesis and chiral organization. *Org. Biomol. Chem.* **2005**, *3*, 3018–3023. [[CrossRef](#)]
6. Kovačević, M.; Kodrin, I.; Cetina, M.; Kmetič, I.; Murati, T.; Čakić Semenčić, M.; Roca, S.; Barišić, L. The conjugates of ferrocene-1,1'-diamine and amino acids. A novel synthetic approach and conformational analysis. *Dalton Trans.* **2015**, *44*, 16405–16420. [[CrossRef](#)]
7. Van Staveren, D.R.; Metzler-Nolte, N. Bioorganometallic Chemistry of Ferrocene. *Chem. Rev.* **2004**, *104*, 5931–5985. [[CrossRef](#)]

8. Tharamani, C.N.; Mahmoud, K.A.; Vasanthakumar, G.R.; Kraatz, H.-B. Studies into the interaction of a ferrocene-conjugates of Gly-Gly-Arg-Tyr with papain: AC voltammetry, impedance spectroscopy and surface plasmon resonance studies. *Sens. Actuators B Chem.* **2009**, *137*, 253–258. [[CrossRef](#)]
9. Kerman, K.; Kraatz, H.-B. Electrochemical probing of HIV enzymes using ferrocene-conjugated peptides on surfaces. *Analyst* **2009**, *134*, 2400–2404. [[CrossRef](#)]
10. Kovačević, M.; Kodrin, I.; Roca, S.; Molčanov, K.; Shen, Y.; Adhikari, B.; Kraatz, H.-B.; Barišić, L. Helically Chiral Peptides That Contain Ferrocene-1,1'-diamine Scaffolds as a Turn Inducer. *Chem. Eur. J.* **2017**, *23*, 10372–10395. [[CrossRef](#)]
11. Scully, C.C.G.; Jensen, P.; Rutledge, P.J. Mercury binding by ferrocenyl peptides with sulfur-containing side chains: Electrochemical, spectroscopic and structural studies. *J. Organomet. Chem.* **2008**, *693*, 2869–2876. [[CrossRef](#)]
12. Qing, G.-Y.; Sun, T.-L.; Wang, F.; He, Y.-B.; Yang, X. Chromogenic Chemosensors for N-Acetylaspartate Based on Chiral Ferrocene-Bearing Thiourea Derivatives. *Eur. J. Org. Chem.* **2009**, *6*, 841–849. [[CrossRef](#)]
13. Moriuchi, T.; Yoshida, K.; Hirao, T. Chirality-Organized Ferrocene Receptor Bearing Podand Dipeptide Chains (–L-Ala-L-Pro-NHPyMe) for the Selective Recognition of Dicarboxylic Acids. *Org. Lett.* **2003**, *5*, 4285–4288. [[CrossRef](#)]
14. Zong, Z.; Cao, Z.; Hao, A.; Xing, P. Dynamic axial chirality of ferrocene diamino acids: Hydration effects and chiroptical applications. *J. Mater. Chem. C* **2021**, *9*, 12191–12200. [[CrossRef](#)]
15. Albada, B.; Metzler-Nolte, N. Highly Potent Antibacterial Organometallic Peptide Conjugates. *Acc. Chem. Res.* **2017**, *50*, 2510–2518. [[CrossRef](#)]
16. Costa, N.C.S.; Piccoli, J.P.; Santos-Filho, N.A.; Clementino, L.C.; Fusco-Almeida, A.M.; De Annunzio, S.R.; Fontana, C.R.; Verga, J.B.M.; Eto, S.F.; Pizauro-Junior, J.M.; et al. Antimicrobial activity of RP-1 peptide conjugate with ferrocene group. *PLoS ONE* **2020**, *15*, e0228740. [[CrossRef](#)]
17. Wenzel, M.; Chiriac, A.I.; Otto, A.; Zweytick, D.; May, C.; Schumacher, C.; Gust, R.; Albada, H.B.; Penkova, M.; Krämer, U.; et al. Small cationic antimicrobial peptides delocalize peripheral membrane proteins. *Proc. Natl. Acad. Sci. USA* **2014**, *111*, 1409–1418. [[CrossRef](#)]
18. Ardila-Chantré, N.; Hernández-Cardonab, A.K.; Pineda-Castañeda, H.M.; Estupiñan-Torresb, S.M.; Leal-Castroc, A.L.; Fierro-Medina, R.; Rivera-Monroy, Z.J.; García-Castañeda, J.E. Short peptides conjugated to non-peptidic motifs exhibit antibacterial activity. *RSC Adv.* **2020**, *10*, 29580–29586. [[CrossRef](#)]
19. Slootweg, J.C.; Prochnow, P.; Bobersky, S.; Bandow, J.E.; Metzler-Nolte, N. Exploring Structure-Activity Relationships in Synthetic Antimicrobial Peptides (synAMPs) by a Ferrocene Scan. *Eur. J. Inorg. Chem.* **2017**, *2*, 360–367. [[CrossRef](#)]
20. Khelef, A.; Lanez, T. In vitro assays of the antioxidant activities of ferrocene derivatives bearing amine, amide or hydrazine groups. *Der Pharma Chem.* **2015**, *7*, 318–323. [[CrossRef](#)]
21. Milaeva, E.R.; Filimonova, S.I.; Meleshonkova, N.N.; Dubova, L.G.; Shevtsova, E.F.; Bachurin, S.O.; Zefirov, N.S. Antioxidative Activity of Ferrocenes Bearing 2,6-Di-Tert-Butylphenol Moieties. *Bioinorg. Chem. Appl.* **2010**, *2010*, 165482. [[CrossRef](#)] [[PubMed](#)]
22. Štimac, A.; Lapić, J.; Blasina, V.; Lukinac, M.; Djaković, S.; Crnolatac, I.; Frkanec, L.; Frkanec, R. Adamantyl ferrocene derivatives: Antioxidant abilities and effects on model lipid membranes. *Appl. Organomet. Chem.* **2017**, *32*, e4042. [[CrossRef](#)]
23. Erckes, V.; Steuer, C. A story of peptides, lipophilicity and chromatography-back and forth in time. *RSC Med. Chem.* **2022**, *13*, 676–687. [[CrossRef](#)] [[PubMed](#)]
24. Lee, A.C.; Harris, J.L.; Khanna, K.K.; Hong, J.H. A Comprehensive Review on Current Advances in Peptide Drug Development and Design. *Int. J. Mol. Sci.* **2019**, *20*, 2383. [[CrossRef](#)] [[PubMed](#)]
25. Wei, C.-W.; Peng, Y.; Zhang, L.; Huang, Q.; Cheng, M.; Liu, Y.-N.; Li, J. Synthesis and evaluation of ferrocenyl pentapeptide (Fc-KLVFF) as an inhibitor of Alzheimer's A β _{1–42} fibril formation in vitro. *Bioorg. Med. Chem. Lett.* **2011**, *21*, 5818–5821. [[CrossRef](#)]
26. Zhou, B.; Li, C.-L.; Hao, Y.-Q.; Johnny, M.C.; Liu, Y.-N.; Li, J. Ferrocene tripeptide Gly-Pro-Arg conjugates: Synthesis and inhibitory effects on Alzheimer's A β _{1–42} fibrillogenesis and A β -induced cytotoxicity in vitro. *Bioorg. Med. Chem.* **2013**, *21*, 395–402. [[CrossRef](#)]
27. Chen, Y.; Yang, C.; Li, T.; Zhang, M.; Liu, Y.; Gauthier, M.A.; Zhao, Y.; Wu, C. The Interplay of Disulfide Bonds, α -Helicity, and Hydrophobic Interactions Leads to Ultrahigh Proteolytic Stability of Peptides. *Biomacromolecules* **2015**, *16*, 2347–2355. [[CrossRef](#)]
28. Porter, E.A.; Weisblum, B.; Gellman, S.H. Mimicry of host-defense peptides by unnatural oligomers: Antimicrobial beta-peptides. *J. Am. Chem. Soc.* **2002**, *124*, 7324–7330. [[CrossRef](#)]
29. Singh, A.; Lumb, I.; Mehrac, V.; Kumar, V. Ferrocene-appended pharmacophores: An exciting approach for modulating the biological potential of organic scaffolds. *Dalton Trans.* **2019**, *48*, 2840–2860. [[CrossRef](#)]
30. Sharma, B.; Kumar, V. Has Ferrocene Really Delivered Its Role in Accentuating the Bioactivity of Organic Scaffolds? *J. Med. Chem.* **2021**, *64*, 16865–16921. [[CrossRef](#)]
31. Kovačević, M.; Molčanov, K.; Radošević, K.; Srček Gaurina, V.; Roca, S.; Čače, A.; Barišić, L. Conjugates of 1'-aminoferrocene-1-carboxylic acid and proline: Synthesis, conformational analysis and biological evaluation. *Molecules* **2014**, *21*, 12852–12880. [[CrossRef](#)]
32. Kovačević, M.; Čakić Semenčić, M.; Radošević, K.; Molčanov, K.; Roca, S.; Šimunović, L.; Kodrin, I.; Barišić, L. Conformational Preferences and Antiproliferative Activity of Peptidomimetics Containing Methyl 1'-Aminoferrocene-1-carboxylate and Turn-Forming Homo- and Heterochiral Pro-Ala Motifs. *Int. J. Mol. Sci.* **2021**, *22*, 13532. [[CrossRef](#)]
33. Čakić Semenčić, M.; Barišić, L. Ferrocene Bioconjugates. *Croat. Chem. Acta* **2017**, *90*, 537–569. [[CrossRef](#)]
34. Idrees, M.; Mohammad, A.R.; Karodia, N.; Rahman, A. Multimodal Role of Amino Acids in Microbial Control and Drug Development. *Antibiotics* **2020**, *9*, 330. [[CrossRef](#)]

35. van de Waterbeemd, H.; Karajiannis, H.; El Tayar, N. Lipophilicity of amino acids. *Amino Acids* **1994**, *7*, 129–145. [[CrossRef](#)]
36. Kovačević, M.; Markulin, D.; Zelenika, M.; Marjanović, M.; Lovrić, M.; Polančec, D.; Ivančić, M.; Mrvčić, J.; Molčanov, K.; Milašinović, V.; et al. Hydrogen Bonding Drives Helical Chirality via 10-Membered Rings in Dipeptide Conjugates of Ferrocene-1,1'-Diamine. *Int. J. Mol. Sci.* **2022**, *23*, 12233. [[CrossRef](#)]
37. Iqbal, M.; Balaram, P. The 310 helical conformation of the amino terminal decapeptide of suzukacillin. 270 MHz hydrogen-1 NMR evidence for eight intramolecular hydrogen bonds. *J. Am. Chem. Soc.* **1981**, *103*, 5548–5552. [[CrossRef](#)]
38. Venkatachalapathi, Y.V.; Prasad, B.V.V.; Balaram, P. Conformational analysis of small disulfide loops. Spectroscopic and theoretical studies on a synthetic cyclic tetrapeptide containing cystine. *Biochemistry* **1982**, *2*, 5502–5509. [[CrossRef](#)]
39. Stevens, E.S.; Sugawara, N.; Bonora, G.M.; Toniolo, C. Conformational analysis of linear peptides. 3. Temperature dependence of NH chemical shifts in chloroform. *J. Am. Chem. Soc.* **1980**, *102*, 7048–7050. [[CrossRef](#)]
40. Patti, A.; Pedotti, S.; Mazzeo, G.; Longhi, G.; Abbate, S.; Paoloni, L.; Bloino, J.; Rampino, S.; Barone, V. Ferrocenes with simple chiral substituents: An in-depth theoretical and experimental VCD and ECD study. *Phys. Chem. Chem. Phys.* **2019**, *21*, 9419–9432. [[CrossRef](#)]
41. Nuskol, M.; Šutalo, P.; Đaković, M.; Kovačević, M.; Kodrin, I.; Čakić Semenčić, M. Testing the Potential of the Ferrocene Chromophore as a Circular Dichroism Probe for the Assignment of the Screw-Sense Preference of Tripeptides. *Organometallics* **2021**, *40*, 1351–1362. [[CrossRef](#)]
42. Čakić Semenčić, M.; Kodrin, I.; Barišić, L.; Nuskol, M.; Meden, A. Synthesis and Conformational Study of Monosubstituted Aminoferrocene-Based Peptides Bearing Homo- and Heterochiral Pro-Ala Sequences. *Eur. J. Inorg. Chem.* **2017**, *2*, 306–317. [[CrossRef](#)]
43. Barišić, L.; Kovačević, M.; Mamić, M.; Kodrin, I.; Mihalić, Z.; Rapić, V. Synthesis and Conformational Analysis of Methyl N-Alanyl-1'-aminoferrocene-1-carboxylate. *Eur. J. Inorg. Chem.* **2012**, *11*, 1810–1822. [[CrossRef](#)]
44. Čakić Semenčić, M.; Kovač, V.; Kodrin, I.; Barišić, L.; Rapić, V. Synthesis and Conformational Study of Bioconjugates Derived from 1-Acetyl-1'-aminoferrocene and α -Amino Acids. *Eur. J. Inorg. Chem.* **2015**, *1*, 112–123. [[CrossRef](#)]
45. Lapić, J.; Djaković, S.; Kodrin, I.; Mihalić, Z.; Cetina, M.; Rapić, V. Preparation and Conformation Analysis of N-(Ferrocenoyl)Dipeptide Esters and Their 1'-Acetyl Derivatives. *Eur. J. Org. Chem.* **2010**, *13*, 2512–2524. [[CrossRef](#)]
46. Kovačević, M.; Rapić, V.; Lukač, I.; Molčanov, K.; Kodrin, I.; Barišić, L. Novel Fully Protected Muramic Acid: A Facile Synthesis and Structural Study. *J. Mol. Struct.* **2013**, *1048*, 349–356. [[CrossRef](#)]
47. Djaković, S.; Kodrin, I.; Smrečki, V.; Novak, P.; Mihalić, Z.; Žihor, D.; Lapić, J.; Rapić, V. 1'-Acetylferrocene Amino Acid Esters and Amides. A Simple Model for Parallel β -Helical Peptides. *Tetrahedron* **2014**, *70*, 2330–2342. [[CrossRef](#)]
48. Nuskol, M.; Studen, B.; Meden, A.; Kodrin, I.; Čakić Semenčić, M. Tight Turn in Dipeptide Bridged Ferrocenes: Synthesis, X-ray Structural, Theoretical and Spectroscopic Studies. *Polyhedron* **2019**, *161*, 137–144. [[CrossRef](#)]
49. Nuskol, M.; Šutalo, P.; Kodrin, I.; Semenčić, M.Č. Sensing of the Induced Helical Chirality by the Chiroptical Response of the Ferrocene Chromophore. *Eur. J. Inorg. Chem.* **2022**, *2*, e202100880. [[CrossRef](#)]
50. Kovač, V.; Kodrin, I.; Radošević, K.; Molčanov, K.; Adhikari, B.; Kraatz, H.-B.; Barišić, L. Oxalamide-Bridged Ferrocenes: Conformational and Gelation Properties and In Vitro Antitumor Activity. *Organometallics* **2022**, *41*, 920–936. [[CrossRef](#)]
51. Čakić Semenčić, M.; Kodrin, I.; Molčanov, K.; Kovačević, M.; Rapić, V. Novel Ferrocene Imide Derivatives: Synthesis, Conformational Analysis and X-ray Structure. *Heliyon* **2022**, *8*, e09470. [[CrossRef](#)]
52. Farrugia, L.J. ORTEP-3 for Windows—a version of ORTEP-III with a Graphical User Interface (GUI). *J. Appl. Cryst.* **1997**, *30*, 565. [[CrossRef](#)]
53. Boto, A.; Pérez de la Lastra, J.M.; González, C.C. The Road from Host-Defense Peptides to a New Generation of Antimicrobial Drugs. *Molecules* **2018**, *23*, 311. [[CrossRef](#)]
54. Zhang, J.; Fu, Y.; Yang, P.; Liu, X.; Li, Y.; Gu, Z. ROS Scavenging Biopolymers for Anti-Inflammatory Diseases: Classification and Formulation. *Adv. Mater. Interfaces* **2020**, *7*, 2000632. [[CrossRef](#)]
55. Lee, T.H.; Hall, K.N.; Aguilar, M.I. Antimicrobial peptide structure and mechanism of action: A focus on the role of membrane structure. *Curr. Top. Med. Chem.* **2016**, *6*, 25–39. [[CrossRef](#)]
56. Li, J.; Koh, J.J.; Liu, S.; Lakshminarayanan, R.; Verma, C.S.; Beuerman, R.W. Membrane active antimicrobial peptides: Translating mechanistic insights to design. *Front. Neurosci.* **2017**, *11*, 73. [[CrossRef](#)]
57. Schmidtchen, A.; Pasupuleti, M.; Malmsten, M. Effect of hydrophobic modifications in antimicrobial peptides. *Adv. Colloid Interface Sci.* **2014**, *205*, 265–274. [[CrossRef](#)]
58. Kataoka, H. Sample Preparation for Liquid Chromatography. In *Liquid Chromatography: Applications*, 2nd ed.; Fanali, S., Haddad, P., Poole, C., Riekkola, M.-L., Eds.; Elsevier: Amsterdam, The Netherlands, 2017; pp. 1–37.
59. Fekete, S.; Veuthey, J.L.; Guillaume, D. New trends in reversed-phase liquid chromatographic separations of therapeutic peptides and proteins: Theory and applications. *J. Pharm. Biomed. Anal.* **2012**, *69*, 9–27. [[CrossRef](#)]
60. Neuhaus, C.S.; Gabernet, G.; Steuer, C.; Hiss, J.A.; Zenobi, R.; Schneider, G. Simulated Molecular Evolution for Anticancer Peptide Design. *Angew. Chem. Int. Ed.* **2019**, *58*, 1674–1678. [[CrossRef](#)]
61. Shibue, M.; Mant, C.T.; Hodges, R.S. Effect of anionic ion-pairing reagent hydrophobicity on selectivity of peptide separations by reversed-phase liquid chromatography. *J. Chromatogr. A* **2005**, *1080*, 68–75. [[CrossRef](#)]
62. Frederiksen, N.; Hansen, P.R.; Björkling, F.; Franzyk, H. Peptide/Peptoid Hybrid Oligomers: The Influence of Hydrophobicity and Relative Side-Chain Length on Antibacterial Activity and Cell Selectivity. *Molecules* **2019**, *24*, 4429. [[CrossRef](#)] [[PubMed](#)]

63. Pirisinu, M.; Blasco, P.; Tian, X.; Sen, Y.; Bode, A.M.; Liu, K.; Dong, Z. Analysis of hydrophobic and hydrophilic moments of short penetrating peptides for enhancing mitochondrial localization: Prediction and validation. *FASEB J.* **2019**, *33*, 7970–7984. [[CrossRef](#)]
64. Medina-Alarcón, K.P.; Singulani, J.L.; Voltan, A.R.; Sardi, J.C.O.; Petrônio, M.S.; Santos, M.B.; Polaquini, C.R.; Regasini, L.O.; Bolzani, V.S.; da Silva, D.H.S.; et al. Alkyl Protocatechuate-Loaded Nanostructured Lipid Systems as a Treatment Strategy for *Paracoccidioides brasiliensis* and *Paracoccidioides lutzii* In Vitro. *Front. Microbiol.* **2017**, *8*, 1048–1060. [[CrossRef](#)] [[PubMed](#)]
65. Pace, C.N.; Fu, H.; Fryar, K.L.; Landua, J.; Trevino, S.R.; Schell, D.; Thurlkill, R.L.; Imura, S.; Scholtz, J.M.; Gajiwala, K.; et al. Contribution of hydrogen bonds to protein stability. *Protein Sci.* **2014**, *23*, 652–661. [[CrossRef](#)] [[PubMed](#)]
66. Lu, J.; Xu, H.; Xia, J.; Ma, J.; Xu, J.; Li, Y.; Feng, J. D- and Unnatural Amino Acid Substituted Antimicrobial Peptides with Improved Proteolytic Resistance and Their Proteolytic Degradation Characteristics. *Front. Microbiol.* **2020**, *11*, 563030. [[CrossRef](#)]
67. Schrödinger, LLC. *MacroModel*; Schrödinger, LLC: New York, NY, USA, 2019.
68. Mohamadi, F.; Richards, N.G.J.; Guida, W.C.; Liskamp, R.; Lipton, M.; Caufield, C.; Chang, G.; Hendrickson, T.; Still, W.C. Macromodel—An integrated software system for modeling organic and bioorganic molecules using molecular mechanics. *J. Comput. Chem.* **1990**, *11*, 440–467. [[CrossRef](#)]
69. Frisch, M.J.; Trucks, G.W.; Schlegel, H.B.; Scuseria, G.E.; Robb, M.A.; Cheeseman, J.R.; Scalmani, G.; Barone, V.; Petersson, G.A.; Nakatsuji, H.; et al. *Gaussian 16*, revision C.01; Gaussian, Inc.: Wallingford, CT, USA, 2016.
70. Becke, A.D. Density-functional thermochemistry. III. The role of exact exchange. *J. Chem. Phys.* **1993**, *98*, 5648–5652. [[CrossRef](#)]
71. Lee, C.; Yang, W.; Parr, R.G. Development of the Colle-Salvetti correlation-energy formula into a functional of the electron density. *Phys. Rev. B* **1998**, *37*, 785–789. [[CrossRef](#)]
72. Grimme, S.; Antony, J.; Ehrlich, S.; Krieg, H. A consistent and accurate ab initio parameterization of density functional dispersion correction (DFT-D) for the 94 elements H-Pu. *J. Chem. Phys.* **2010**, *132*, 154104. [[CrossRef](#)]
73. Marenich, A.V.; Cramer, C.J.; Truhlar, D.G. Universal solvation model based on solute electron density and a continuum model of the solvent defined by the bulk dielectric constant and atomic surface tensions. *J. Phys. Chem. B* **2009**, *113*, 6378–6396. [[CrossRef](#)]
74. Keith, T.A. *AIMAll*, version 19.02.13; TK Gristmill Software: Overland Park, KS, USA, 2017.
75. Koch, U.; Popelier, P.L.A. Characterization of C-H-O Hydrogen Bonds on the Basis of the Charge Density. *J. Phys. Chem.* **1995**, *99*, 9747–9754. [[CrossRef](#)]
76. Rigaku Corporation. *CrysAlis*, version 1.171.42.69a; Rigaku Oxford Diffraction Ltd.: Yarnton, UK, 2022.
77. Sheldrick, G.M. SHELXT-integrated space-group and crystal-structure determination. *Acta Crystallogr. A Found. Adv.* **2015**, *71*, 3–8. [[CrossRef](#)]
78. Sheldrick, G.M. Crystal structure refinement with SHELXL. *Acta Crystallogr. C* **2015**, *71*, 3–8. [[CrossRef](#)]
79. Farrugia, L.J. WinGX and ORTEP for Windows: An update. *J. Appl. Cryst.* **2012**, *45*, 849–854. [[CrossRef](#)]
80. Spek, A.L. CheckCIF validation ALERTS: What they mean and how to respond. *Acta Crystallogr.* **2020**, *76*, 1–11. [[CrossRef](#)]
81. Macrae, C.F.; Sovago, I.; Cottrell, S.J.; Galek, P.T.A.; McCabe, P.; Pidcock, E.; Platings, M.; Shields, G.P.; Stevens, J.S.; Towler, M.; et al. Mercury 4.0: From visualization to analysis, design and prediction. *J. Appl. Cryst.* **2020**, *53*, 226–235. [[CrossRef](#)]
82. Balouiri, M.; Sadiki, M.; Ibsouda, S.K. Methods for in vitro evaluating antimicrobial activity: A review. *J. Pharm. Anal.* **2016**, *6*, 71–79. [[CrossRef](#)]

Disclaimer/Publisher’s Note: The statements, opinions and data contained in all publications are solely those of the individual author(s) and contributor(s) and not of MDPI and/or the editor(s). MDPI and/or the editor(s) disclaim responsibility for any injury to people or property resulting from any ideas, methods, instructions or products referred to in the content.